A Proof-of-Concept for Epigenetic Therapy of Tissue Fibrosis: Inhibition of Liver Fibrosis Progression by 3-Deazaneplanocin A

Müjdat Zeybel,[1,7,8] Saimir Luli,[1,8] Laura Sabater,[1] Timothy Hardy,[1] Fiona Oakley,[1] Jack Leslie,[1] Agata Page,[1] Eva Moran Salvador,[1] Victoria Sharkey,[1] Hidekazu Tsukamoto,[2,3] David C.K. Chu,[4] Uma Sharan Singh,[4] Mirco Ponzoni,[5] Patrizia Perri,[5] Daniela Di Paolo,[5] Edgar J. Mendivil,[6] Jelena Mann,[1] and Derek A. Mann[1]

[1]Institute of Cellular Medicine, Faculty of Medical Sciences, 4th Floor, William Leech Building, Newcastle University, Framlington Place, Newcastle upon Tyne, NE2 4HH, UK; [2]Southern California Research Center for ALPD and Cirrhosis, Keck School of Medicine, University of Southern California, Los Angeles, CA 90033, USA; [3]Department of Veterans Affairs, Greater Los Angeles Healthcare System, Los Angeles, CA 90033, USA; [4]The University of Georgia College of Pharmacy, Athens, GA 30602, USA; [5]Experimental Therapy Unit, Laboratory of Oncology, Istituto Giannina Gaslini, 16148 Genova, Italy; [6]Department of Molecular Biology and Genomics, Institute for Molecular Biology and Gene Therapy, University of Guadalajara, 44100 Guadalajara, Mexico; [7]School of Medicine, Koc University, 34450 Istanbul, Turkey

The progression of fibrosis in chronic liver disease is dependent upon hepatic stellate cells (HSCs) transdifferentiating to a myofibroblast-like phenotype. This pivotal process is controlled by enzymes that regulate histone methylation and chromatin structure, which may be targets for developing anti-fibrotics. There is limited pre-clinical experimental support for the potential to therapeutically manipulate epigenetic regulators in fibrosis. In order to learn if epigenetic treatment can halt the progression of pre-established liver fibrosis, we treated mice with the histone methyltransferase inhibitor 3-deazaneplanocin A (DZNep) in a naked form or by selectively targeting HSC-derived myofibroblasts via an antibody-liposome-DZNep targeting vehicle. We discovered that DZNep treatment inhibited multiple histone methylation modifications, indicative of a broader specificity than previously reported. This broad epigenetic repression was associated with the suppression of fibrosis progression as assessed both histologically and biochemically. The anti-fibrotic effect of DZNep was reproduced when the drug was selectively targeted to HSC-derived myofibroblasts. Therefore, the in vivo modulation of HSC histone methylation is sufficient to halt progression of fibrosis in the context of continuous liver damage. This discovery and our novel HSC-targeting vehicle, which avoids the unwanted effects of epigenetic drugs on parenchymal liver cells, represents an important proof-of-concept for epigenetic treatment of liver fibrosis.

INTRODUCTION

Fibrosis is a pathology associated with aging, chronic disease, and a variety of connective tissue disorders, including arthritis, systemic scleroderma, and athrofibrosis.[1] The development of fibrosis in a tissue arises from remodelling of connective tissue and the net deposition of a collagen-rich fibril-forming extracellular matrix (ECM). Fibrotic remodelling is often a progressive process culminating in architectural and functional disruption of the affected tissue; in the case of vital tissues, such as the liver, lung, heart, or kidney, fibrosis may lead to organ dysfunction and early mortality. Fibrosis also establishes microenvironments in which cancers are more likely to emerge, an example being liver fibrosis and/or cirrhosis, which is a major risk factor for hepatocellular carcinoma.[2] At the present time, there is a lack of clinically proven effective antifibrotic drugs; the exception being Pirfenidone, now approved for treatment of idiopathic pulmonary fibrosis.[3] There is, therefore, an urgent need to develop novel therapeutic strategies that either suppress fibrosis or promote fibrosis regression.

Myofibroblasts are the major cell type responsible for deposition and maintenance of the fibrotic ECM irrespective of the tissue type or the underlying cause of damage.[4,5] The majority of myofibroblasts are generated locally in response to tissue injury, which usually occurs via the transdifferentiation of precursor cells, such as pericytes or resident fibroblasts, or by the process of epithelial-to-mesenchymal transition.[6,7] A normal wound healing response is self-limiting to enable subsequent tissue regeneration, and this response is associated with clearance of myofibroblasts by apoptosis or reversal of transdifferentiation.[8–10] However, in the context of repeated tissue injury or unresolved chronic inflammation, myofibroblasts persist and establish autocrine signaling pathways that stimulate their survival, proliferation, migration, and continued production of fibrotic ECM. The persistence of tissue myofibroblasts is a common feature of progressive fibrosis and a major driver of disease progression.[4] Furthermore, myofibroblasts within the fibrotic matrix can be

CrossMark

"activated" toward a highly proinflammatory state in response to epithelial stress; this indicates that fibrosis-associated myofibroblasts become orchestrators of inflammation within the diseased tissue.[11] Myofibroblasts are therefore key therapeutic targets in fibrosis, but a major challenge is to identify safe and efficacious drug targets that selectively modulate myofibroblast biology.

Transdifferentiation of resident liver sinusoidal hepatic stellate cells (HSCs) into myofibroblasts is tightly regulated by epigenetic modifications, including relandscaping of the DNA methylome and chromatin remodelling at genes regulating the myofibroblast phenotype.[12–14] EZH2 is the catalytic component of the polycomb repressor 2 complex responsible for methylation of histone 3 lysine 27 (H3K27) and is required for stimulating enrichment of the repressive H3K27me3 mark.[14] Enrichment of H3K27me3 at the PPARγ gene is a fundamental epigenetic modification during HSC transdifferentiation that brings about transcriptional repression of PPARγ; this is an essential step for the cell to acquire its myofibroblastic phenotype. Indeed, forced expression of PPARγ in liver myofibroblasts is sufficient to repress collagen expression and reprogram the HSC phenotype to resemble its precursor quiescent state.[15] Small-molecule inhibitors of EZH2, including GSK126, EPZ-6438, and 3-deazaneplanocin A (DZNep), have been proposed for therapeutic development in cancer.[16–18] We have previously reported in vitro experiments that show that DZNep can irreversibly suppress classic morphological and biochemical changes associated with HSC transdifferentiation.[14] Similar studies in lung myofibroblasts have confirmed that inhibition of EZH2 suppresses their fibrogenic phenotype and decreases collagen production.[19] However, the potential for in vivo inhibition of EZH2 as an antifibrotic strategy has not been determined.

In a well-established in vivo model of HSC transdifferentiation and liver fibrosis, we show that therapeutic administration of DZNep in the context of pre-established liver disease is able to effectively suppress progression of fibrosis despite continued liver damage. Moreover, we have developed an antibody-liposome-targeting vehicle that can specifically deliver encapsulated molecules to liver myofibroblasts.[20] Incorporation of targeting antibody into the surface liposome is a novel approach that further develops liposomal technology that was previously used to deliver agents for experimental treatment of liver fibrosis.[21–24] We demonstrate that in vivo application of this novel targeting approach achieves selective inhibition of the H3K27me3 mark in myofibroblasts and halts progression of fibrosis. Our findings provide an exciting proof-of-concept for the use of emerging epigenetic drugs in the treatment of fibrosis in chronic disease and highlight the therapeutic potential of targeting EZH2 and potentially other profibrogenic histone lysine methyltransferases (HKMTs).

RESULTS

DZNep and Related Purine Analogs Suppress Induction of Type I Collagen Expression

DZNep is a purine nucleoside analog (PNA), which is in a family of compounds, many of which are being used clinically and have been proven to be effective in the treatment of hematological malignancies and autoimmune disorders.[33] In a blinded fashion, we began by determining the ability of several chemically-related PNAs (designated compounds 1–9; Figure S1) to inhibit HSC expression of transcripts for the profibrogenic genes collagen 1A1, αSMA, and TIMP-1. This experiment was carried out in vitro using the widely adopted cell-culture model of HSC transdifferentiation in which freshly isolated primary rodent HSCs are cultured for several days in complete serum-containing media. In this model, HSCs undergo a similar process of transdifferentiation to that described in vivo, which serves as a robust tool for pre-clinical drug discovery.[34] The drugs were added to HSCs that had been freshly isolated from normal rat liver and cultured on plastic in complete serum-containing media for just 1 day, at which point the cells had not yet undergone transdifferentiation. Based on results from our previous studies, the compounds were tested at a single concentration of 1 μg/mL in each case. After a further 6 days, at which point HSCs had adopted the myofibroblast phenotype, cultures were harvested and was RNA isolated for qRT-PCR analyses of gene expression. Compounds 3, 4, 5, and 8 were found to repress collagen 1A1 gene expression; compounds 1 and 3 repressed αSMA gene expression, while compound 2 showed the overall best antifibrogenic performance by inhibiting collagen 1A1, αSMA, and TIMP1 gene expression (Figures 1A–1C). Decoding the experiment revealed that compound 2 was DZNep which, in addition to suppressing expression of all three fibrogenic genes, was confirmed to prevent cultured HSCs from adopting the morphology of an activated myofibroblast (Figure 1D). Furthermore, culturing of quiescent HSCs (qHSCs) in the presence of DZNep resulted in increased apoptosis in day 7 cells (Figures 1E and 1F, left panel) while also reducing proliferation (Figure 1F, right panel). These data indicate that PNAs are a class of compounds with strong potential for antifibrotic activities and confirm that DZNep is a molecule worthy of in vivo investigations.

DZNep Prevents the Progression of Carbon Tetrachloride-Induced Liver Fibrosis

Repetitive exposure of the liver to the hepatotoxin carbon tetrachloride (CCl_4) establishes repeated rounds of liver damage and inflammation, which drives a progressive fibrogenic process chiefly mediated by the activities of myofibroblasts generated from an HSC origin.[10] To determine the in vivo antifibrotic properties of DZNep, adult male C57Bl6 mice were injured with CCl_4 for 2 weeks in order to establish mild fibrosis and were subsequently therapeutically administered DZNep (or vehicle control) over a further 6 weeks while being continually injured with CCl_4 (Figure 2A) Sirius Red staining of liver sections (Figure 2B) and morphometric analysis (Figure 2C) showed the expected progressive accumulation of cross-linked fibril-forming collagens between weeks 2 and 8. Remarkably, this disease progression was attenuated in mice treated with DZNep (Figures 2B and 2C). Staining for αSMA again revealed the expected time-dependent increase in the numbers of myofibroblasts when comparing the 2- and 8-week control groups; however, DZNep treatment prevented this accumulation of scar-forming myofibroblasts (Figures 2D and 2E). There were no significant changes in the number
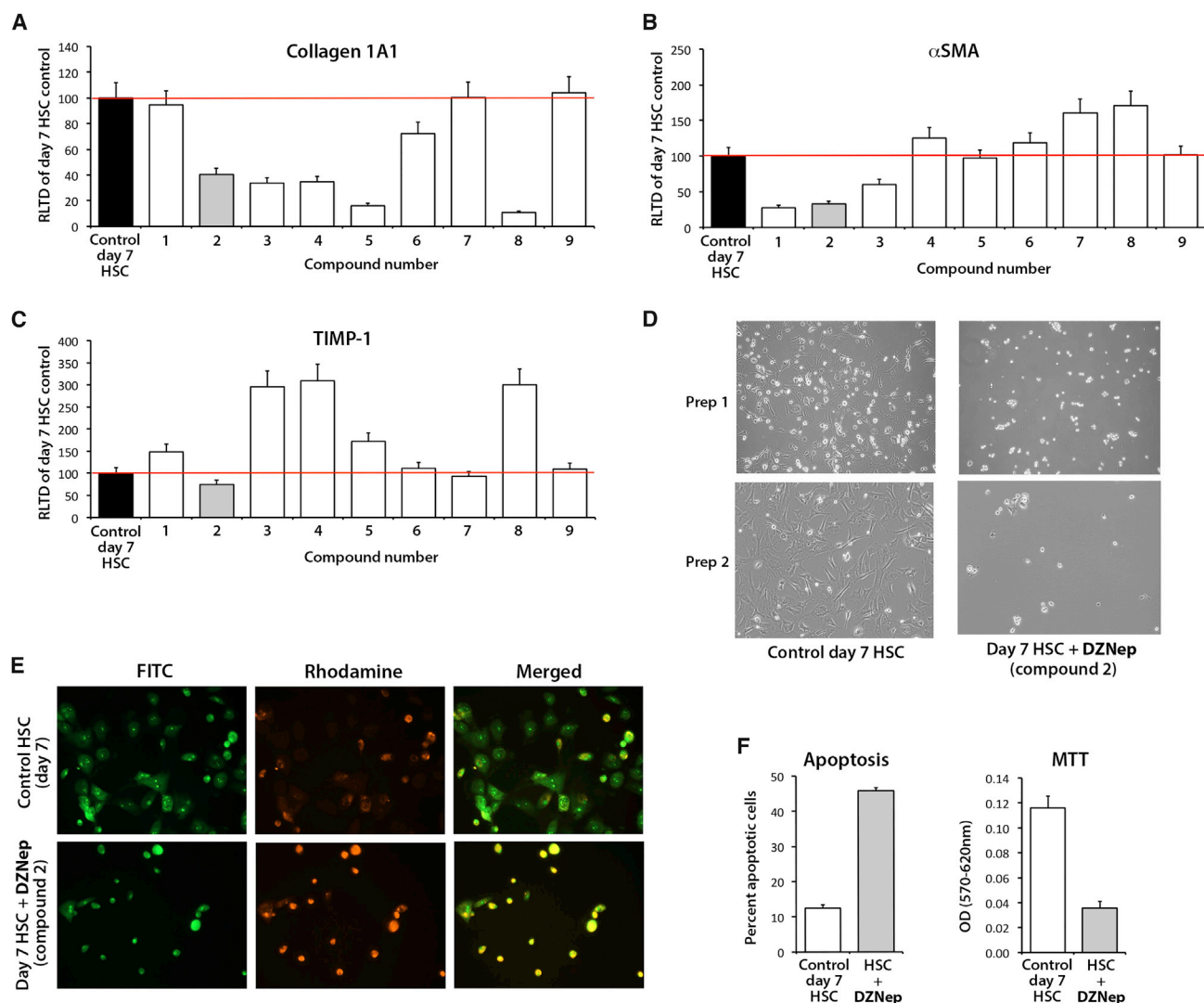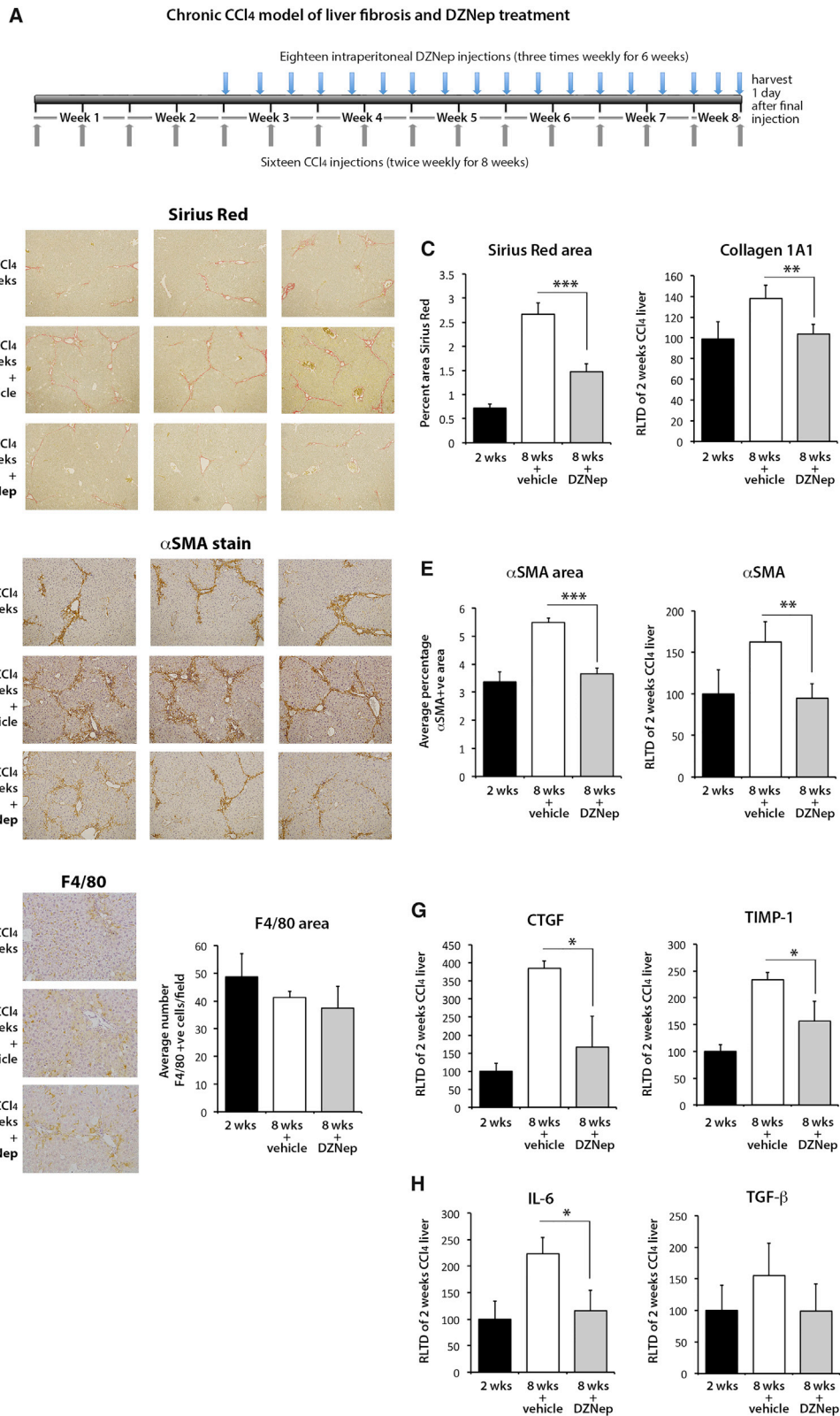
Figure 1. Purine Nucleoside Analogs Demonstrate Varied Ability to Inhibit HSC Transdifferentiation In Vitro

(A–C) Freshly isolated rat HSCs were grown for 7 days in the presence of 1 μg/mL each of a series of chemically related PNAs (designated compounds 1–9). The cells were harvested on day 7, and transcripts for collagen I (A), αSMA (B), and TIMP-1 (C) were quantified by qPCR in at least four separate preparations of HSCs. The best-performing drug across all assays is in gray (compound 2). The line on the bar graphs shows the level of gene expression in control cells. Error bars represent mean ± SEM. RLTD, relative level of transcriptional difference. (D) Representative photomicrographs showing morphological differences between day 7 control-activated HSCs or equivalent culture grown in the presence of 1 μg/mL compound 2 (deazaneplanocin A). (E) Representative FITC (left), rhodamine (middle), and merged (right) fluorescent images of acridine orange-stained day 7 control-activated HSCs or equivalent culture grown in the presence of 1 μg/mL compound 2 (deazaneplanocin A). (F) Graphs showing average percentage of apoptotic cells (left panel) and number of proliferating cells (MTT assay, right panel).

of macrophages observed between the groups (Figure 2F). Quantification of hepatic transcripts at 8 weeks confirmed the anticipated time-dependent increases in expression of fibrogenic collagen 1A1 (Figure 2C), αSMA (Figure 2E), CTGF, TIMP-1 (Figure 2G), IL-6, and transforming growth factor β1 (TGF-β1) (Figure 2H) in control mice. By contrast, in DZNep-treated mice, levels of these transcripts were similar to those measured at 2 weeks, thus reflecting the repressive effect of the drug on accumulation of αSMA+ cells. There were no significant changes in expression of vascular endothelial growth fac-

tor (VEGF) or angiopoetin 1 in any of the groups (Figure S2). To ascertain broader effects of DZNep on gene expression, we carried out an unbiased microarray analysis of the hepatic transcriptome comparing the 8-week vehicle control group to the DZNep-treated group (Figure 3). DZNep increased the expression of 248 genes and decreased expression of 108 genes (Tables S1 and S3). The heatmap in Figure 3A shows replicates for the top 15 most upregulated and downregulated genes, while Figures 3B and 3C provide validatory qRT-PCRs for a subset of the downregulated and upregulated genes,

A   Chronic CCl4 model of liver fibrosis and DZNep treatment

Eighteen intraperitoneal DZNep injections (three times weekly for 6 weeks)

harvest 1 day after final injection

Sixteen CCl4 injections (twice weekly for 8 weeks)

B   Sirius Red

Chronic CCl4 2 weeks

Chronic CCl4 8 weeks + vehicle

Chronic CCl4 8 weeks + DZNep

C Sirius Red area

Collagen 1A1

D   αSMA stain

E αSMA area

αSMA

F   F4/80

F4/80 area

G CTGF

TIMP-1

H IL-6

TGF-β

(legend on next page)

respectively. Of particular note, among the downregulated genes were Acta2 (αSMA) and CTGF, confirming the qRT-PCR data; the transcription factor EGR1 was also downregulated, which plays a core role in fibrogenesis by positively regulating the expression of multiple fibrogenic growth factors, including TGF-β1, platelet-derived growth factor (PDGF), and fibroblast growth factor (FGF).[35] Strongly upregulated genes were enriched for those encoding enzymes involved in the metabolism of xenobiotics or bile acids (Cyp2c37, Cyp2c50, Cyp7a1, Cyp8b1, and Inmt), lipids (Acss2 and Thrsp1), iron (Hamp2), and glucose (G6Pc). However, alanine transaminase (ALT) values were not significantly different between the control of DZNep-treated groups, indicating that the drug does not display any obvious hepatotoxicity over and above that caused by CCl4 and, further, that the observed changes in expression of metabolic genes did not cause any interference with CCl4-induced liver damage (Figures S3A and S3B). Notably, expression of Cyp2E1, which metabolises CCl4 in the liver, remained unchanged in this model (Figure S4).

DZNep Acts as a Broad Specificity Inhibitor of Hepatic Histone Methyltransferases

To confirm that the antifibrogenic activity of DZNep was associated with the expected in vivo repression of the H3K27me3 epigenetic mark controlled by EZH2, we carried out western blotting using protein extracts from 8-week vehicle control and DZNep-treated livers. Relative to vehicle controls, a loss of hepatic H3K27me3 was associated with DZNep treatment in the CCl4 models (Figure 4A). However, we also observed a loss of other histone modifications, including epigenetic marks associated with transcriptional activation (H3K36me3 and H3K4me3) and repression (H3K9me3) (Figure 4A). These data support previous results, indicating a broader effect of DZNep on histone lysine methyltransferase activities than suggested in earlier reports, which claimed specificity of the drug for EZH2.[18] Furthermore, free DZNep was repressing H3K27 trimethyation in multiple hepatic cell types in addition to HSCs, including hepatocytes and cholangiocytes (Figure 4B).

Targeting of DZNep to HSC-Derived Myofibroblasts Inhibits Fibrosis

Given the broad inhibitory effects of DZNep on histone lysine methyltransferases (HKMTs) and the suggestion from hepatic mRNA expression data of potential metabolic effects on hepatocytes, it was plausible that the observed anti-fibrotic activities of the drug might not reflect a direct activity in HSCs. To address this important caveat,

we exploited recent advances in liposome-mediated drug delivery, ligand-mediated cell targeting of liposomes, and the specificity of the single chain antibody (ScAb) C1-3 for HSC-derived myofibroblasts.[36,37] C1-3 specifically recognizes synaptophysin, a transmembrane protein that is selectively expressed on HSC-derived myofibroblasts in the diseased liver.[38] We therefore asked if targeted delivery of DZNep to HSC-derived myofibroblasts in C1-3-coated liposomes could bring about a similar therapeutic effect as that observed with free DZNep. Prior to answering this question, we first confirmed the specificity of C1-3-liposome conjugates for liver myofibroblasts. To this end, the cytotoxic drug doxyrubicin (Dox) was incorporated into liposomes as detailed in the Materials and Methods (and summarized in Figure S5). Dox-liposomes were subsequently separated from free Dox by purification over a Sephadex G50 column. Critically, the Dox-liposome complexes were constructed from lipid conjugates, which included a DSPE-PEG$_{2000}$-MAL group in which the maleimide terminus could be used for coupling to targeting proteins.[26] We exploited this chemistry to couple Dox-liposomes to C1-3 or a control (CSBD9) ScAb, the latter lacking specificity for myofibroblasts. ScAb-Dox-liposomes were then administered to mice undergoing acute injury with a high dose of CCl4 in which HSCs were stimulated to undergo myofibroblast transdifferentiation (Figure 5A). Relative to control liposomes, C1-3-Dox-liposomes had no effect on CCl4-induced serum ALT, AST, and ALP values, indicating no obvious impact on hepatocyte death (Figure S6). C1-3-Dox-liposomes had no effect on the number of hepatic macrophages, neutrophils, or proliferating hepatocytes (Figures 5B–5D). In contrast, livers of C1-3-Dox-liposomes had roughly half the number of αSMA+ myofibroblasts compared with controls (Figure 5E), and this was associated with reduced hepatic expression of TGF-β1 (Figure 5F). These data provided us with confidence that C1-3-liposomes provide an effective vehicle for in vivo delivery of encapsulated drugs selectively to HSC-derived myofibroblasts. We next generated C1-3-DZNep-liposomes together with a control vehicle CSBD9-DZNep-liposomes. To determine the in vivo therapeutic potential of DZNep-liposome-C1-3 conjugates, they were administered to mice under a similar experimental CCl4 therapeutic model as previously described for free DZNep. Mice were initially injured for 2 weeks to establish liver disease, prior to a further 6 weeks of injury, during which time the animals were administered either C1-3-DZNep-liposomes or control CSBD9-DZNep-liposomes (Figure 6A). After 8 weeks, mice were culled, and all liver sections were stained with Sirius red for collagen and by immunohistochemistry for αSMA (Figures 6B and 6C). As shown in Figures 6B and 6C, significantly less

Figure 2. DZNep Prevents Fibrosis Progression in a Chronic Model of CCl4-Induced Liver Fibrosis
(A) Schematic representation of chronic CCl4 model of liver fibrosis combined with progressive therapeutic treatment with DZNep. Grey arrows show frequency of CCl4 injections, whereas blue arrows show DZNep injections. Briefly, liver fibrosis was established for 2 weeks followed by administration of DZNep treatment alongside CCl4 for a further 6 weeks. (B) Histological sections showing collagen staining (Sirius Red). (C) Graphs showing average percentage area for Sirius Red (left) and mRNA levels of Collagen 1A1 as quantified by qPCR in livers from all animals in the study (right). (D) αSMA staining in three representative control or DZNep-treated animals as well as the animals at the starting point of treatment (2 weeks CCl4). (E) Graphs showing average percentage area αSMA in all groups (left) and mRNA levels of αSMA as quantified by qPCR in livers (right). (F) Histological sections showing macrophage staining (F4/80, left panels) and graphs showing average number of F4/80 positive cells per field (right panel). (G) mRNA levels for ΧΤΓΦ, TIMΠ−1, (H) IΛ−6, and ΤΓΦβ1 as quantified by qPCR in livers of all animals. Error bars in relevant panels represent mean ± SEM. *p < 0.05; **p < 0.01; ***p < 0.001.
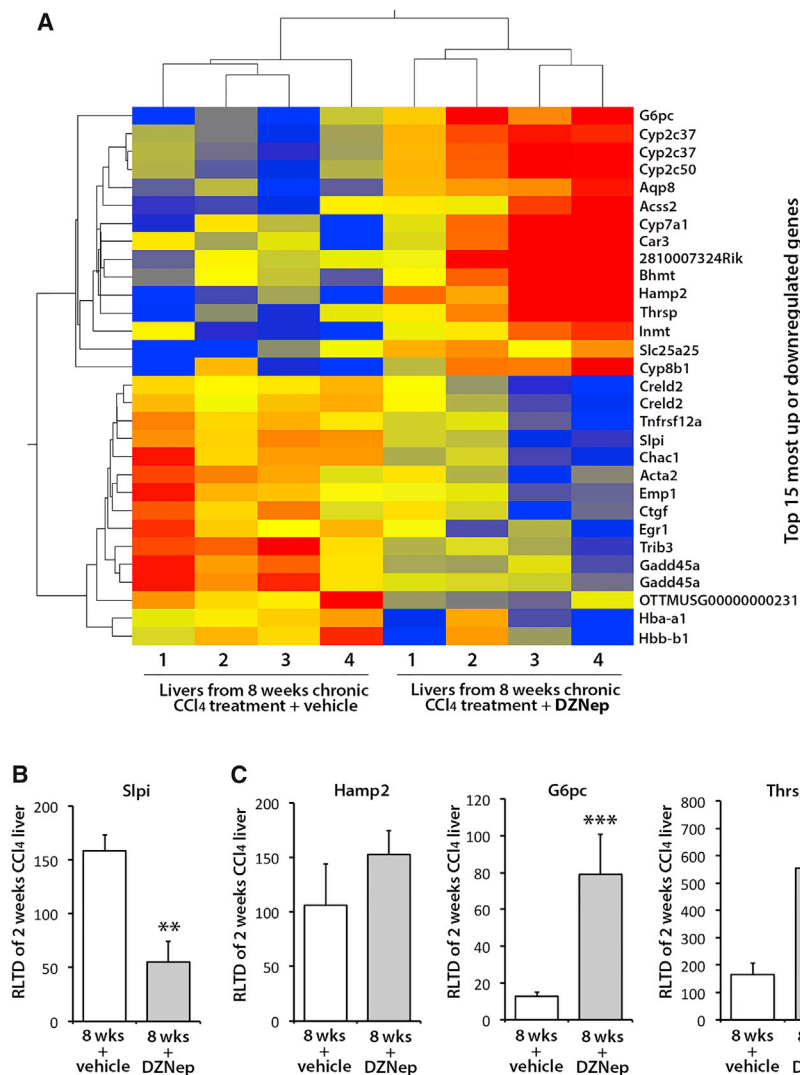
A

B

C

Figure 3. DZNep Alters Expression of Numerous Genes in a Chronic Model of CCl4-Induced Liver Fibrosis

(A) A heatmap displaying results of microarray carried out using four control and four DZNep-treated livers from a chronic model of CCl_4-induced liver fibrosis. The top 15 most upregulated and downregulated genes are shown. Blue, negative values (i.e., downregulated); red, positive (upregulated); yellow, unchanged. (B) mRNA level of Slpi and (C) Hamp2, G6pc, and Thrsp genes was quantified by qPCR in order to validate the results of microarray. Error bars in relevant panels represent mean ± SEM. **p < 0.01; ***p < 0.001.

of H3K27me3 staining only in myofibroblasts in the livers of mice receiving C1-3-DZNep-liposomes, while mice treated with control CSBD9-DZNep-liposomes showed the presence of H3K27me3 in all cell types, including myofibroblasts (Figure 7A). Dual immunofluorescence staining of livers for αSMA and H3K27me3 further confirmed that treatment with C1-3-DZNep-liposomes is associated with selective loss of the epigenetic mark in myofibroblasts (Figure 7B).

DISCUSSION

The concept of epigenetic therapy is now well-established in the field of oncology, with the successful clinical application of inhibitors of DNA methylation (e.g., decitabine) and histone deacetylases (e.g., SAHA) described for many types of cancers.[39] Akin to cancer, fibrosis is a pathology that is associated with dramatic changes in tissue architecture underpinned by alterations in cell differentiation, fate, and function. In particular, the generation, proliferation, and lifespan of myofibroblasts, the major cellular drivers of extracellular matrix deposition, are important determinants of fibrosis progression.[40] Chronic disease is often characterized by an unresolved wound-healing process in which tissue myofibroblasts are continually produced and become highly proliferative, motile, and resistant to apoptosis.[8,40] The behavioral parallels of myofibroblasts to those of neoplastic cells, in particular, their proliferative nature and resistance to apoptosis, have led our group and other investigators to explore the possibility that epigenetic alterations may regulate their phenotype and behavior and, in turn, the course of the fibrogenic process.[41] Transdifferentiation of HSCs represents the major cellular source of myofibroblasts in chronic liver disease and is associated with global changes in gene expression underpinned by re-landscaping of the HSC epigenome, including genome-wide changes in DNA methylation and histone modifications.[12,13,42] Previous in vitro studies and a small number of in vivo studies have demonstrated the ability of pharmacological inhibitors of DNA methylation, histone deacetylation, and histone

fibrotic collagen accumulated in the livers of mice receiving C1-3-DZNep-liposomes compared with those treated with control CSBD9-DZNep-liposomes. This difference in fibrosis was reflected in associated levels of hepatic αSMA, which were lower in livers of C1-3-DZNep-liposome recipients (Figure 6C, right panel). Targetted DZNep also resulted in a significant reduction of collagen 1A1, CTGF, and angiopoetin 1 expression (Figure 6D), while no change was detected in the expression of TIMP1 (Figure S7). We conclude that in vivo targeting of DZNep to HSCs using a C1-3-liposome vehicle leads to a reduction in the number of hepatic myofibroblasts in diseased livers, suppression of collagen deposition, and reduced levels of hepatic fibrosis.

To show specificity of C1-3-DZNep-liposome treatment for hepatic myofibrobalsts, we stained the livers of C1-3-DZNep-liposomes and control CSBD9-DZNep-liposomes for the presence of an H3K27me3 epigenetic mark (Figure 7A). Data showed the absence
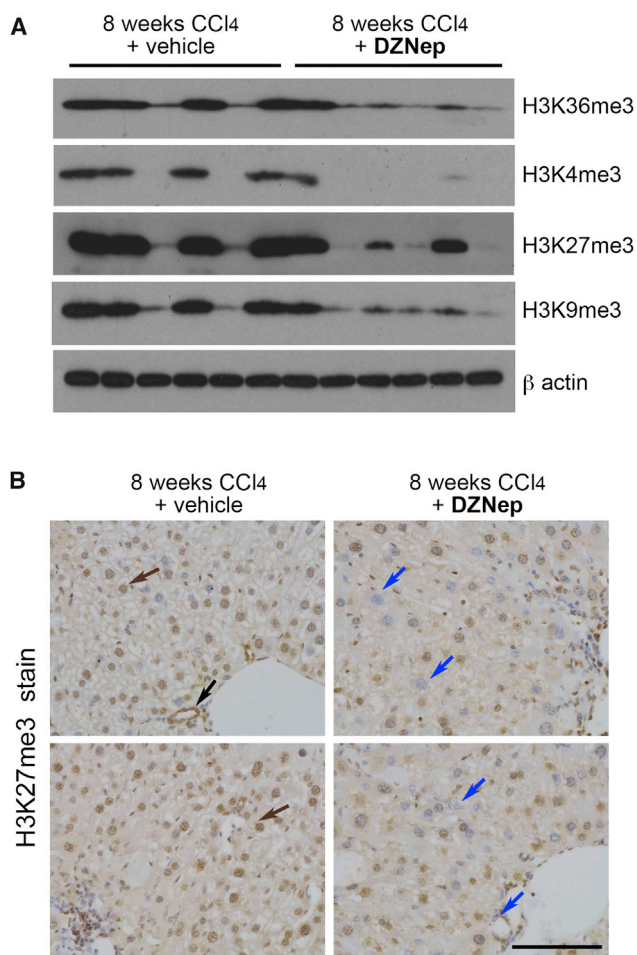
A

B

Figure 4. DZNep Inhibition of Histone Methylation Is Not Specific to H3K27me3

(A) 30 μg whole-cell protein from six livers of control animals or six livers from DZNep-treated livers within the chronic model of CCl₄-induced liver fibrosis were immunoblotted for H3K36me3, H3K4me3, H3K27me3, H3K9me3, and β-actin. (B) Histological sections showing H3K27me3 staining in a representative set of vehicle or DZNep-treated chronic CCl₄ livers. Brown arrows show the presence of H3K27me3 staining in hepatocytes and biliary epithelial cells of vehicle-treated fibrotic livers, with H3K27me3 markedly absent in both cell types in DZNep-treated livers.

methylation to suppress in vivo and culture-induced HSC transdifferentiation as well as development of fibrosis.[12,14,43–47] The potential for epigenetic approaches to be exploited for suppressing fibrosis is also supported by in vivo investigations with mice lacking the master epigenetic regulator MeCP2, which is attenuated for fibrosis across multiple tissues, including liver, lung, heart, and retina.[14,48–52] The work we have described in this present study significantly advances these previous investigations by showing that in vivo administration of the epigenetic drug DZNep halts the progression of pre-established experimental liver fibrosis despite sustained liver damage. Remarkably, we were able to demonstrate that this anti-fibrotic activity of DZNep is retained when the drug is selectively targeted to HSC-derived myofibroblasts, thus providing the first proof-of-concept

that progressive tissue fibrosis can be therapeutically attenuated via the direct epigenetic manipulation of the myofibroblast.

A major target of DZNep is EZH2, the only HKMT in nature that catalyzes trimethylation at H3K27.[53] EZH2 is aberrantly expressed in numerous cancers, including leukemia, pancreatic ductal adenocarcinoma, and hepatocellular carcinoma, and there are now many pre-clinical studies reporting the inhibitory effects of DZNep on tumor growth.[54,55] Treatment of cells with DZNep results in depletion of EZH2 and, as such, this effect and the associated loss of the H3K27me3 mark is considered to be its major mechanism of anti-tumor activity. However, we report that in vivo administration of DZNep has broader inhibitory effects on histone 3 methylation in the liver, with global diminution of H3K4me3, H3K9me3, and H3K36me3 as well as the anticipated loss of H3K27me3. This non-selective effect of DZNep on histone methylation has previously been described using in vitro cancer cell models where the drug suppressed both repressive and active histone methylation marks.[18] On the one hand, a drug such as DZNep, which has a global impact on histone methylation, may be clinically adventitious since HSC transdifferentiation requires the de novo annotation of multiple repressive and activatory histone methylation marks, thus reflecting the need to repress the expression of genes that promote the adipogenic phenotype of quiescent HSCs while simultaneously programming the transcription of genes that are characteristic of the myofibroblast phenotype.[12–14] As an example, de novo expression of MeCP2 is induced shortly after HSCs are plated into culture and leads to the almost simultaneous de novo expression of EZH2 and ASH1 which, combined, stimulate H3K27me3-mediated repression of anti-fibrogenic PPARγ and H3K4me3-regulated transcription of pro-fibrogenic TGF-β1, TIMP-1, and type I collagen I genes.[13,14] On the other hand, a systemic repression of histone methylation in the context of a long-term therapeutic regimen would be likely to result in unwanted side effects, as might the global loss of EZH2 expression. In this regard, DZNep-mediated suppression of EZH2 has been reported to enhance lipid accumulation and inflammation in high-fat diet models of rodent liver disease.[56] One solution to this problem explored here is the use of a myofibroblast-targeting vehicle to achieve in vivo cell-selective delivery of DZNep. This aim was achieved by initially showing that liposomes coated with the HSCs targeting ScAb C1-3 and loaded with the cytotoxic drug doxyrubicin selectively depleted αSMA+ liver myofibroblasts. We then demonstrated that therapeutic administration of C1-3-coated liposomes carrying DZNep halted fibrosis progression in the CCl₄ model with a similar efficacy to that achieved when administering "naked" DZNep. This approach supports our hypothesis that in vivo therapeutic effects of DZNep are a consequence of direct targeting of epigenetic events in liver myofibroblasts rather than being due to effects on other types of liver cells. We propose that this myofibroblast-selective drug delivery technology may be developed for other therapeutic compounds that have the potential to effect a broad number of cell types and, in particular, for epigenetic drugs that modulate chromatin modifications common to more than one type of liver cell. It is important to note that the basic liposome vehicle we have used lends itself to the incorporation of a wide number of therapeutic molecules, including small drug-like
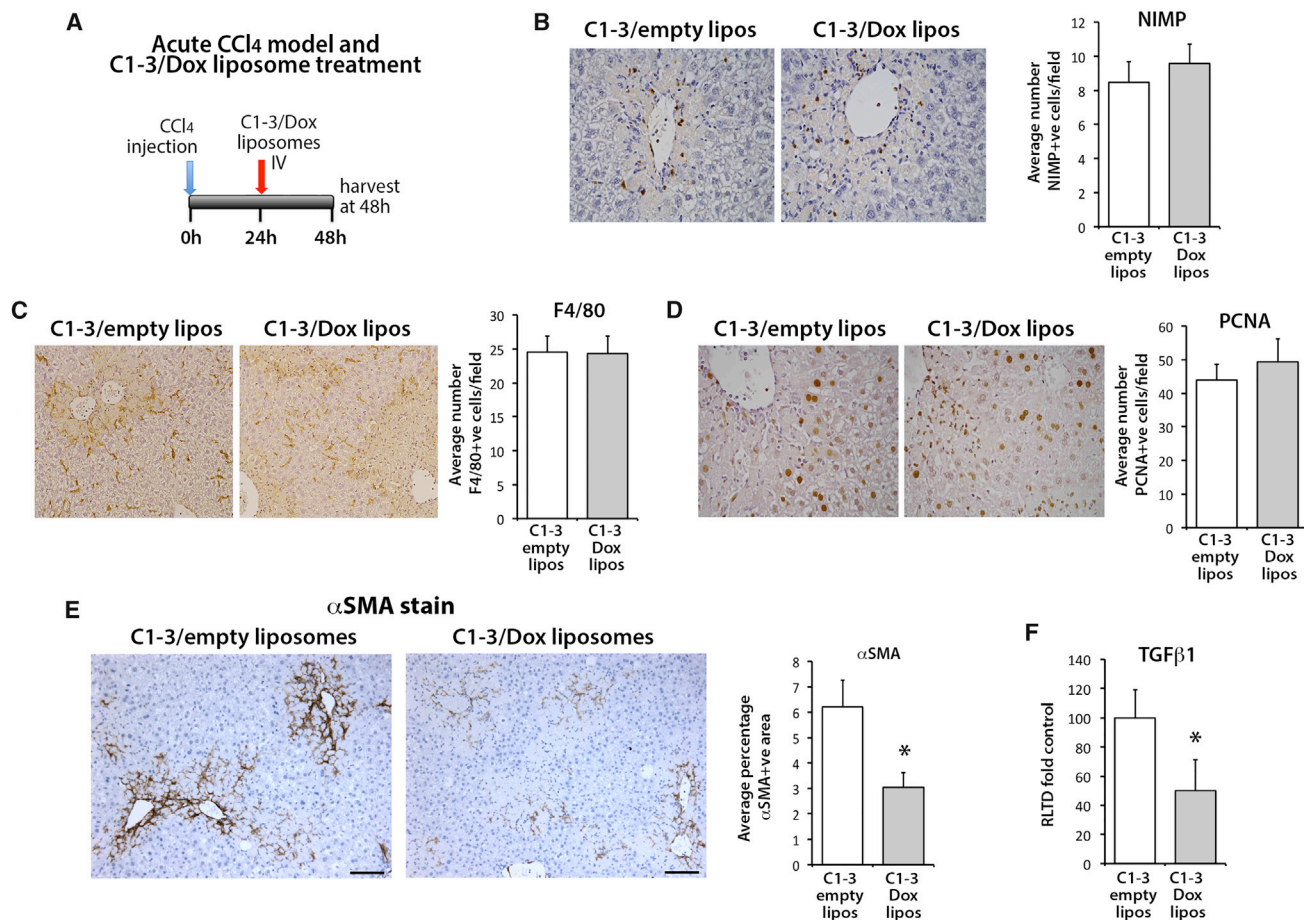
Figure 5. Liposomes Coated with C1-3 ScAb and Loaded with Doxorubicin Significantly Decrease Numbers of Hepatic Myofibroblasts

(A) Schematic representation of acute CCl_4 model of liver fibrosis and therapeutic treatment with C1-3/Dox liposomes. (B) Representative histological sections and graph showing average number of NIMP+ cells (neutrophils), (C) F4/80 (macrophages), and (D) PCNA in control (C1-3/empty liposomes) or C1-3/doxorubicin liposomes treated livers. (E) αSMA staining in representative control (C1-3/empty liposomes) or C1-3/doxorubicin liposome-treated animals and average αSMA positive area in both groups of livers. (F) mRNA levels of TGF-β1 as quantified by qPCR in livers of control (C1-3/empty liposomes) and C1-3/doxorubicin liposome-treated animals. Error bars in relevant panels represent mean ± SEM. *p < 0.05.

compounds, modulatory RNAs and DNAs, antibodies, and peptide-based molecules, all of which can theoretically be encapsulated into the vehicle without the need for chemical modifications. A second solution to the problem of specificity of epigenetic therapeutics that is being actively pursued in both academic and industrial groups is the design of highly selective HKMT inhibitors.[57] It is anticipated that we will shortly have available a toolbox of drug-like molecules that have a high degree of specificity for a particular histone-modifying enzyme. As an example, BIX01294 (BIX) is a potent and selective inhibitor of the G9a and GLP members of the SUV39 family of H3K9 methyltransferases that has been shown to attenuate fibrosis in the experimental unilateral ureteral obstruction (UUO) renal disease model.[58]

In summary, we have used the epigenetic inhibitor DZNep in models of pre-established chronic liver disease to establish the concept that progression of liver fibrosis can be manipulated by the pharmacological targeting of epigenetic modifications in myofibroblasts. With this proof-of-concept, there is now a rational basis for the screening of emerging "epi-drugs" as potential anti-fibrotics for either halting or even reversing the fibrotic process in the absence of an effective treatment for the underlying cause of liver damage.

MATERIALS AND METHODS

Ethics

We hold appropriate licenses for animal experiments, which were issued and/or approved by the local ethical committee and UK Home Office.

Cell Culture

HSCs were isolated from normal livers of 350-g adult male Sprague-Dawley rats by sequential perfusion with collagenase and pronase,

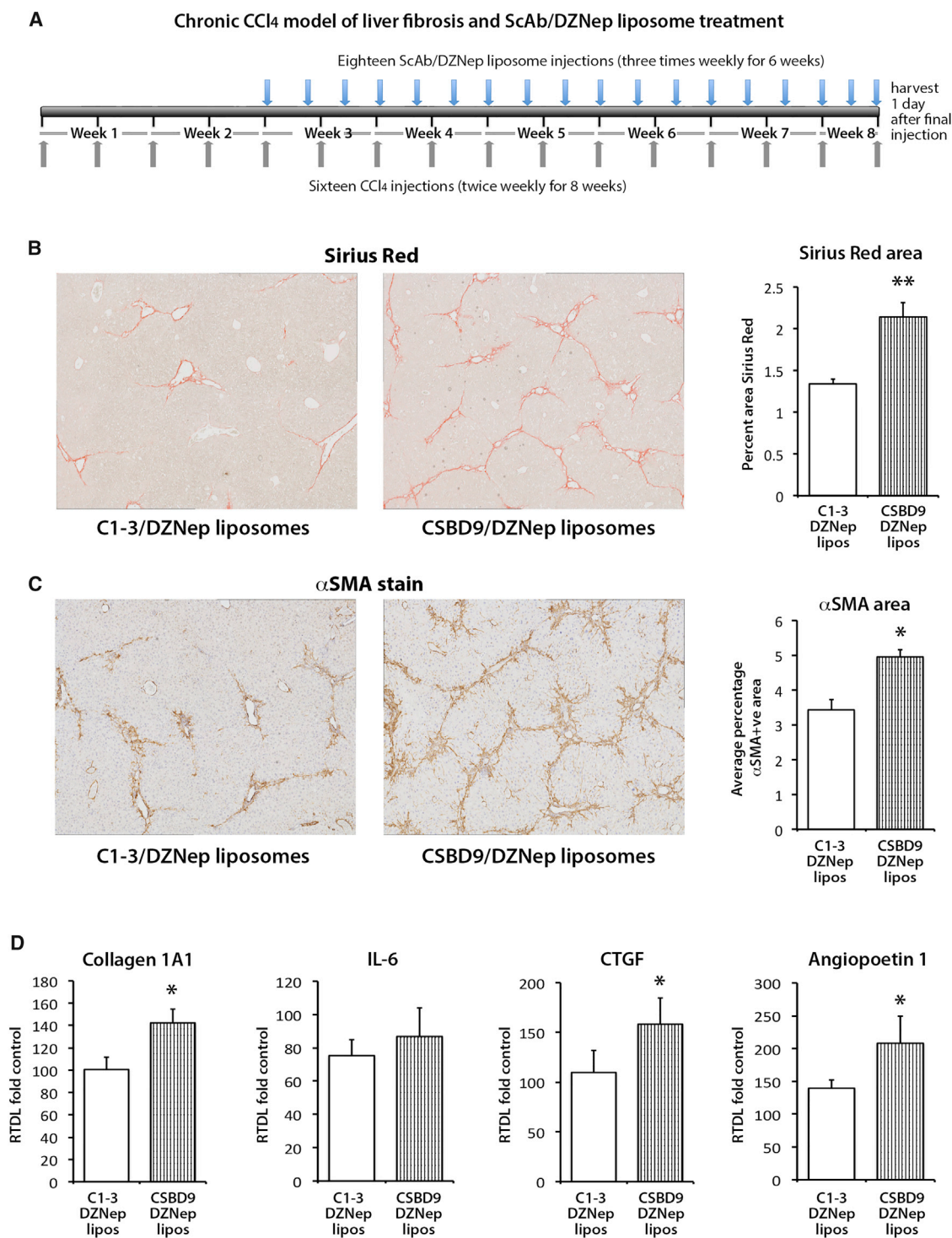**A** **Chronic CCl4 model of liver fibrosis and ScAb/DZNep liposome treatment**

Figure 6. Liposomes Coated with C1-3 ScAb and Loaded with DZNep Significantly Reduce Fibrosis in a Chronic CCl₄ Model of Liver Fibrosis

(A) Schematic representation of the chronic CCl₄ model of liver fibrosis combined with progressive treatment with ScAb/DZNep liposomes. Briefly, liver fibrosis was established for 2 weeks, then the control ScAb CSBD9 or C1-3-coated DZNep-loaded liposomes were administered to animals alongside CCl₄ for a further 6 weeks.

(legend continued on next page)

followed by discontinuous density centrifugation in 11.5% Optiprep (Life Technologies). HSCs were cultured on plastic in DMEM supplemented with penicillin 100 U/mL, streptomycin 100 μg/mL, l-glutamine 2 mmol/L, and 16% fetal calf serum and were maintained at 37°C in an atmosphere of 5% CO_2. Activated HSCs were generated by continuous culture of freshly isolated cells on plastic for 7 days.

Small-Molecule Inhibitors of HSC Activation

Nine proprietary compounds were obtained from D.C.K.C. and tested on day 1 quiescent HSCs in a range of concentrations for their ability to prevent HSC activation in vitro (Figure S1). A concentration of 1 ug/mL was used in the experiments shown. Compounds were applied on quiescent HSCs 12 hr after the isolation, and cells were later harvested at time intervals as indicated.

Histology and/or Immunohistochemistry

Mouse liver tissue was fixed in 10% formalin in PBS, and staining was performed on formalin-fixed paraffin-embedded liver sections. Sirius red staining was performed as previously described.[25] αSMA and H3K27me3 staining was carried out by blocking the endogenous peroxidase activity with 2% hydrogen peroxide in methanol, and then antigen retrieval was achieved using citiric saline antigen unmasking solution (Vector Laboratories). Tissue was blocked using an Avidin/Biotin Blocking Kit (Vector Laboratories) followed by 20% swine serum in PBS and then incubated with primary antibodies; anti-αSMA antibody at 1:1000 (F3777 Sigma) or anti-H3K27 antibody was used at 1:200 (C15410195, diagnode) overnight at 4°C. The next day, slides were PBS washed and then incubated with biotinylated goat anti-fluorescein 1:300 (BA-0601 Vector) or biotinylated swine anti-rabbit 1:200 (eo353 Dako), followed by Vectastain Elite ABC Reagent. Antigens were visualized using a DAB peroxidase substrate kit and counterstained with Mayer's hematoxylin. Slides were imaged using a Nikon ECLIPSE Ni-U (Nikon) microscope, and blinded image analysis of 10 fields at 10× magnification was performed using Nikon Imaging Software Elements Basic Research (NIS-Elements).

For dual αSMA and H3K27me3 staining, slides were treated with citiric saline antigen unmasking solution, then incubated in 0.1% saponin for 10 min. Slides were then PBS washed, blocked with 1× casein and BSA for 60 min, and then incubated with the mouse monoclonal anti-alpha smooth muscle actin FITC conjugated antibodies (Sigma, F3777; dilution factor 1:50) and rabbit anti-H3K27me3 antibodies (dilution factor 1:50) overnight at 4°C. The next morning, slides were PBS washed and incubated with anti-rabbit tetramethylrhodamine (TRITC) secondary Ab (1:100) for 2 hr. Counterstain was performed using 0.3% sudan black in 70% ethanol (EtOH) prior to incubating with DAPI special formulation NucBlue live ready probes

reagent (Life Technologies) for 10 min at room temperature. The slides were then mounted with ProLong Gold antifade reagent (Life Technologies). Images were taken using a Leica TCS SP2 UV AOBS MP confocal microscope.

DZNep Liposomal Preparation

Liposomes were synthetized from HSPC:CHE:DSPE-PEG$_{2000}$: DSPE-PEG2$_{000}$-MAL, 2:1:0.06:0.04 molar ratio, respectively. Lipids were dissolved in chloroform at 10 mM and lipids and DZNep were combined at the molar ratio of 11:1. Subsequently, PBS was added, and the mixture was vortexed and then emulsified by sonication for 5 min (200 W) at 4°C using a probe sonicator (Sonicator-ultrasonic liquid processor XL, Misonix). The mixture was then processed by reverse-phase evaporation using a rota-evaporator (Laborota 4000 Heidolph, Asynt) to remove the organic phase by rotary evaporation under a stream of N_2 until the system reverted to the aqueous phase. Following hydration in PBS, liposomes were extruded (LiposoFast-basic extruder, Avestin) through a series of polycarbonate filters of pore size ranging from 400 nm down to 100 nm. Free DZNep was separated from liposomes by passing liposomes over a Sephadex G-50 column pre-equilibrated in PBS. Finally, C1-3 or CSDB9 single-chain variable fragment (ScFvs) are coupled to the maleimide terminus of DSPE-PEG$_{2000}$-MAL using the previously described methods for whole antibodies and for Fab' fragments coupling with slightly modifications.[26] Briefly, to activate the C1-3 and CSBD9 fragments for reactivity toward the maleimide, we utilized 2-iminothiolane (Traut's reagent) to convert exposed amino groups on the antibody into free sulfhydryl groups. A 20:1 mole ratio of 2-iminothiolane to ScFvs and 1 hr of incubation at room temperature with occasional mixing gave optimal ScFv activation. After separation of thiolated ScFvs from iminothiolane with the use of Sephadex G-25 column chromatography, the ScFv was slowly added to the liposomes in the presence of a small magnetic stirring bar. Oxygen was displaced by running a slow stream of nitrogen over the reaction mixture. The tube was capped and sealed with Teflon tape, and the reaction mixture was incubated overnight at room temperature with continuous slow stirring. The resulting immunoliposomes were separated from unreacted ScFvs by chromatography with the use of Sepharose CL-4B, sterilized by filtration through 0.2-μm pore cellulose membranes (Millipore), and stored at 4°C until use. The antibody density was evaluated by BioRad protein assay.

Particle size (in nanometers), polydispersity index (PdI), and zeta potential (Z-potential in megavolts) of liposomal preparations were measured at 25°C using a Malvern Nano ZS90 light scattering apparatus (Malvern Instruments) at a scattering angle of 90°C.[27–31] The physico-chemical features of this novel delivery system are similar to those obtained in our previously published

(B) Histological sections showing collagen staining (Sirius Red) in a representative control or C1-3/DZNep liposome-treated liver. Right panel: graph showing percent positive area stained with Sirius Red. (C) Histological sections showing αSMA staining in a representative control or C1-3/DZNep liposome-treated liver. Right panel: graph showing percent positive area stained with anti αSMA antibody. (D) mRNA levels of Collagen 1A1, IL-6, CTGF, and angiopoetin 1 as quantified by qPCR in livers of control and C1-3/DZNep liposome-treated animals. Error bars in relevant panels represent mean ± SEM. *p < 0.05, **p < 0.01.
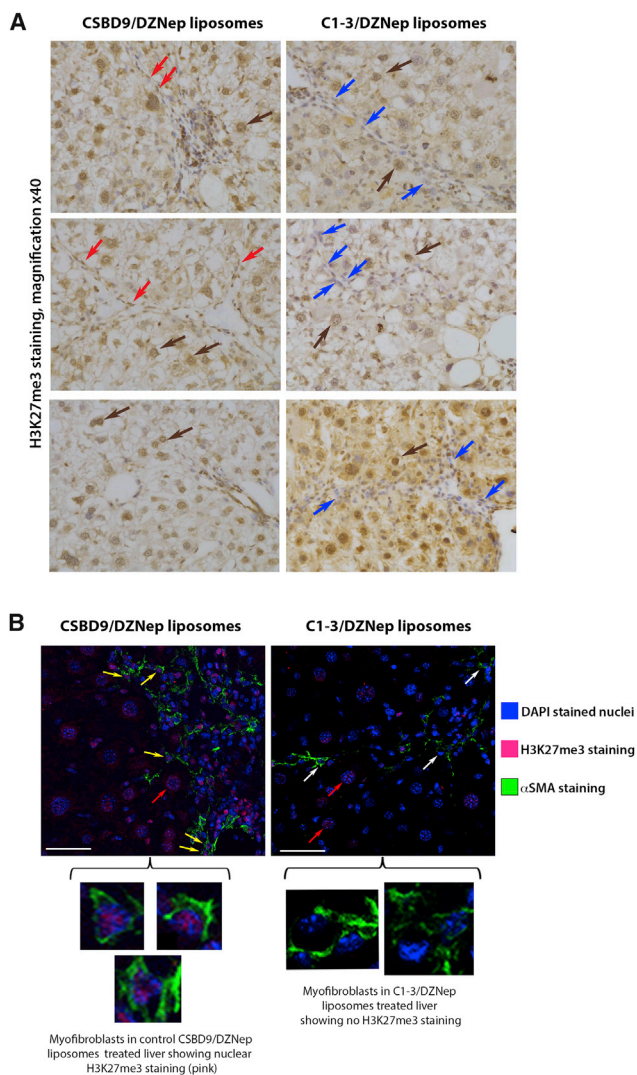
Figure 7. Liposomes Coated with C1-3 ScAb and Loaded with DZNep Reduce the Amount of H3K27me3 Present in Hepatic Myofibroblasts, but Not Hepatocytes

(A) Histological sections showing H3K27me3 staining in a representative set of control CSBD9/DZNep liposomes or C1-3/DZNep liposome-treated chronic CCl_4 livers. Brown arrows, presence of H3K27me3 staining in hepatocytes in both groups; red arrows, presence of H3K27me3 staining in myofibroblasts in CSBD9/DZNep liposome-treated livers; blue arrows, point to myofibroblasts in C1-3/DZNep liposome-treated livers that have lost expression of this hitone mark due to the targeted treatment. (B) Representative images show confocal maximum projections of immunofluorescent-stained liver sections from chronic CCl_4 injured mice treated with CSBD9 or C1-3 coated liposomes, loaded with DZNep at 40× magnification with 1.71 zoom. Sections are stained with DAPI (blue), anti H3K27me3 (red), and anti αSMA (green). Yellow arrows, H3K27me3+ staining (red) in nuclei of αSMA+ cells (green); white arrows, H3K27me3− staining (red) in nuclei of αSMA+ cells (green); red arrows, H3K27me3+ staining in hepatocytes. Scale bars, 43.63 μM.

studies performed with other encapsulated drugs and nucleic acid liposomal formulations,[27–31] thus indicating a possible clinical translation.

Liver Fibrosis In Vivo Models: CCl_4 and Free Drug DZNep Treatment

Chronic CCl_4 was injected intraperitoneally (i.p.) biweekly at 2 μL (CCl_4/olive oil, 1:3 (v/v))/g/body) for 8 weeks. From 2 weeks onward, in addition to CCl_4, mice received 150 mg/kg DZNep or vehicle triweekly by i.p. injection for a further 6 weeks. Twenty-four hours after the final CCl_4 administration, animals were terminated and liver and serum samples were prepared.

Liver Fibrosis In Vivo Models: CCl_4 and Liposomal DZNep Treatment

Chronic CCl_4 was injected intraperitoneally (i.p.) biweekly at 2 μL (CCl_4/olive oil, 1:3 (v/v))/g/body) for 8 weeks. From 2 weeks onward, in addition to CCl_4, mice received 200 μL of liposomal DZNep preparation coated with C1-3 single chain antibody (ScAb) or CSBD9 control ScAb triweekly by intravenous (i.v.) injection for a further 6 weeks. Twenty-four hours after the final CCl_4 administration, animals were terminated and liver and serum samples were prepared.

RNA Isolation and qRT-PCR

Total RNA was isolated from approximately 200 mg of frozen livers or from $\sim 5 \times 10^6$ cultured cells using the Total RNA Purification Kit (QIAGEN). First-strand complementary DNA was generated by using 1 μg of deoxyribonuclease-treated RNA, 1 μL of random hexamer primer (p(dN)$_6$), and ribonuclease-free water (QIAGEN) heated at 70°C for 5 min and then placed on ice. RNasin (ribonuclease inhibitor), 100 U of Moloney murine leukemia virus reverse transcriptase, 1 × Moloney murine leukemia virus buffer, and 0.4 mmol/L deoxynucleoside triphosphates were added, and the mix was incubated at 42°C for 1 hr. SYBR Green qRT-PCR was performed using the primers listed in Table 1.

qPCR

SYBR Green qRT-PCR reactions were performed in a total volume of 13 μL containing 20 ng of cDNA template, 6.5 μL of SYBR Green JumpStart Taq ReadyMix (Sigma), and 20 pmols of forward and reverse primers (Table 1). The PCR reaction was carried out on a 7500 Fast Real-Time PCR System (Applied Biosystem) with the following parameters: 1 cycle at 95°C for 10 s followed by 40 cycles at 95°C for 10 s, 55°C–60°C (primer pair specific annealing temperature, see Tables 1 and S1) for 30 s, and finally 72°C for 30 s. Melt curve analysis was employed to confirm the presence of a single PCR product. All reactions were normalized to rat β-actin or human GAPDH internal control, and the relative level of transcriptional difference was calculated using the $2^{\Delta\Delta Ct}$ method.

Sodium Dodecyl Sulfate: Polyacrylamide Gel Electrophoresis and Immunoblotting

Whole-cell extracts were prepared, and the protein concentration of samples was determined by using a Bradford DC assay kit (Bio-Rad). Whole-cell extracts from samples of interest were then fractionated by electrophoresis through a 9% sodium dodecyl sulfate-polyacrylamide gel. Gels were run at 100 V for 1.5 hr before

Table 1. qPCR Primers

Gene	Forward and Reverse Primer Pair Sequences	Annealing Temperature (°C)
Mouse Collagen 1A1	TTCACCTACAGCACGCTTGTG	58
	GATGACTGTCTTGCCCCAAGTT	
Mouse CTGF	CAAAGCAGCTGCAAATACCA	58
	GGCCAAATGTGTCTTCCAGT	
Mouse TIMP-1	GCAACTCGGACCTGGTCATAA	58
	CGGCCCGTGATGAGAAACT	
Mouse IL-6	GAGGATACCACTCCCAACAGACC	58
	AAGTGCATCATCGTTGTTCATACA	
Mouse TGFβ 1	CTCCCGTGGCTTCTAGTGC	58
	GCCTTAGTTTGGACAGGATCTG	
Mouse α SMA	TCAGCGCCTCCAGTTCCT	58
	AAAAAAAACCACGAGTAACAAATCAA	
Mouse Slpi	GTGGAAGGAGGCAAAAATGA	58
	GACATTGGGAGGGTTAAGCA	
Mouse HAMP2	CTGCCTGTCTCCTGCTTCTC	58
	GCAGATGGGGAAGTTGATGT	
Mouse G6pC	TCTGTCCCGGATCTACCTTG	58
	GTAGAATCCAAGCGCGAAAC	
Mouse Thrsp	ACGGAGCCCCTGATCTCTAT	58
	GGCTTCTAGGTCCAGCTCCT	
Mouse GAPDH	GCACAGTCAAGGCCGAGAAT	58
	GCCTTCTCCATGGTGGTGAA	
Mouse angiopoietin 1	AGGCTTGGTTTCTCGTCAGA	56
	TCTGCACAGTCTCGAAATGG	

transfer onto nitrocellulose. After thr blockade of nonspecific protein binding, nitrocellulose blots were incubated for 1 hr with primary antibodies diluted in Tris-buffered saline (TBS)/Tween 20 (0.075%) containing 5% bovine serum albumin. Rabbit polyclonal antibody-recognizing EZH2 was used at 1/500 dilution (Active Motif, catalog no. 39103), H3K27me2 (Abcam ab24684), H3K27me3 (Abcam, ab6002), H3K4me3 (Abcam, ab8580), and β-actin at 1/1000 dilution (Sigma). After incubation with primary antibodies, blots were washed three times in TBS/Tween 20 before incubation for 1 hr in appropriate horseradish peroxidase-conjugated secondary antibody. After extensive washing in TBS/Tween 20, the blots were processed with distilled water for detection of antigen by using the enhanced chemiluminescence system (Amersham Biosciences).

Microarray

Chronic CCl$_4$ control or DZNep-treated livers (as outlined in the liver fibrosis in vivo models) were used to prepare total RNA, which was utilized for ILMR8 Illumina service MouseRef-8 v2.0 Expression BeadChip. Analysis of microarray data was performed using R from Bioconductor, which has superior normalization specific for illumina arrays (http://www.bioconductor.org/packages/2.10/bioc/html/lumi.html). Following this stage, Rank Prod was used to generate a list of differentially expressed genes. (http://www.bioconductor.org/packages/2.10/bioc/html/RankProd.html).

MTT Assay

Solutions of 3-[4, 5-dimethylthiazol-2-yl]-2, 5-diphenyl tetrazolium bromide (MTT) were dissolved in cell culture medium. HSC treated ± DZNep were seeded at 1×10^5/mL per well in a 12-well tissue culture plate (Greiner) and cultured for 7 days. Cells were PBS washed and then serum starved overnight in 0.1% serum containing media. 100 μL stock of MTT (Sigma) salt (final concentration of 0.5 mg/mL in DPBS) was added to each well for 2 hr at 37°C. Formazan crystals formed were solubilized using 800 μL isopropanol with gentle agitation at room temperature; 200 μL from each well was transferred into a flat bottomed 96 well dish and then quantified using a spectrophotometric plate reader at 570 nm/620 nm and analyzed with SoftMax Pro software.

Quantification of Apoptosis

Apoptotic cells were identified and counted by acridine orange staining and counted as previously described.[32] Acridine orange emits green fluorescence when bound to double-stranded DNA (dsDNA) in the FITC channel and red fluorescence when bound to single-stranded DNA (ssDNA) or RNA in the Rhodamine channel. Images were taken at 10× magnification using a Zeiss axio observer D.1.

Statistical Analysis

Data are expressed as mean ± SEM. All p values were calculated using a two-tailed paired or unpaired Student t test. Statistically significant data are represented in figures where *$p < 0.05$, **$p < 0.01$, and ***$p < 0.001$, respectively.

SUPPLEMENTAL INFORMATION

Supplemental Information includes seven figures and two tables and can be found with this article online at http://dx.doi.org/10.1016/j.ymthe.2016.10.004.

AUTHOR CONTRIBUTIONS

CONFLICTS OF INTEREST

The authors who have taken part in this study declare that they do not have anything to disclose regarding funding or conflict of interest with respect to this manuscript.

REFERENCES

1. Rockey, D.C., Bell, P.D., and Hill, J.A. (2015). Fibrosis–A Common Pathway to Organ Injury and Failure. N. Engl. J. Med. 373, 96.

2. Llovet, J.M., and Bruix, J. (2008). Novel advancements in the management of hepatocellular carcinoma in 2008. J. Hepatol. 48 (Suppl 1), S20–S37.

3. Azuma, A., Nukiwa, T., Tsuboi, E., Suga, M., Abe, S., Nakata, K., Taguchi, Y., Nagai, S., Itoh, H., Ohi, M., et al. (2005). Double-blind, placebo-controlled trial of pirfenidone in patients with idiopathic pulmonary fibrosis. Am. J. Respir. Crit. Care Med. 171, 1040–1047.

4. Gabbiani, G. (2003). The myofibroblast in wound healing and fibrocontractive diseases. J. Pathol. 200, 500–503.

5. Hinz, B., Phan, S.H., Thannickal, V.J., Galli, A., Bochaton-Piallat, M.L., and Gabbiani, G. (2007). The myofibroblast: one function, multiple origins. Am. J. Pathol. 170, 1807–1816.

6. Schrimpf, C., and Duffield, J.S. (2011). Mechanisms of fibrosis: the role of the pericyte. Curr. Opin. Nephrol. Hypertens. 20, 297–305.

7. Guarino, M., Tosoni, A., and Nebuloni, M. (2009). Direct contribution of epithelium to organ fibrosis: epithelial-mesenchymal transition. Hum. Pathol. 40, 1365–1376.

8. Elsharkawy, A.M., Oakley, F., and Mann, D.A. (2005). The role and regulation of hepatic stellate cell apoptosis in reversal of liver fibrosis. Apoptosis 10, 927–939.

9. Kisseleva, T., Cong, M., Paik, Y., Scholten, D., Jiang, C., Benner, C., Iwaisako, K., Moore-Morris, T., Scott, B., Tsukamoto, H., et al. (2012). Myofibroblasts revert to an inactive phenotype during regression of liver fibrosis. Proc. Natl. Acad. Sci. USA 109, 9448–9453.

10. Mederacke, I., Hsu, C.C., Troeger, J.S., Huebener, P., Mu, X., Dapito, D.H., Pradere, J.P., and Schwabe, R.F. (2013). Fate tracing reveals hepatic stellate cells as dominant contributors to liver fibrosis independent of its aetiology. Nat. Commun. 4, 2823.

11. Suwara, M.I., Green, N.J., Borthwick, L.A., Mann, J., Mayer-Barber, K.D., Barron, L., Corris, P.A., Farrow, S.N., Wynn, T.A., Fisher, A.J., and Mann, D.A. (2014). IL-1α released from damaged epithelial cells is sufficient and essential to trigger inflammatory responses in human lung fibroblasts. Mucosal Immunol. 7, 684–693.

12. Page, A., Paoli, P., Moran Salvador, E., White, S., French, J., and Mann, J. (2016). Hepatic stellate cell transdifferentiation involves genome-wide remodeling of the DNA methylation landscape. J. Hepatol. 64, 661–673.

13. Perugorria, M.J., Wilson, C.L., Zeybel, M., Walsh, M., Amin, S., Robinson, S., White, S.A., Burt, A.D., Oakley, F., Tsukamoto, H., et al. (2012). Histone methyltransferase ASH1 orchestrates fibrogenic gene transcription during myofibroblast transdifferentiation. Hepatology 56, 1129–1139.

14. Mann, J., Chu, D.C., Maxwell, A., Oakley, F., Zhu, N.L., Tsukamoto, H., and Mann, D.A. (2010). MeCP2 controls an epigenetic pathway that promotes myofibroblast transdifferentiation and fibrosis. Gastroenterology 138, 705–714, 714.e1–e4.

15. Hazra, S., Xiong, S., Wang, J., Rippe, R.A., Krishna, V., Chatterjee, K., and Tsukamoto, H. (2004). Peroxisome proliferator-activated receptor gamma induces a phenotypic switch from activated to quiescent hepatic stellate cells. J. Biol. Chem. 279, 11392–11401.

16. McCabe, M.T., Ott, H.M., Ganji, G., Korenchuk, S., Thompson, C., Van Aller, G.S., Liu, Y., Graves, A.P., Della Pietra, A., 3rd, Diaz, E., et al. (2012). EZH2 inhibition as a therapeutic strategy for lymphoma with EZH2-activating mutations. Nature 492, 108–112.

17. Knutson, S.K., Kawano, S., Minoshima, Y., Warholic, N.M., Huang, K.C., Xiao, Y., Kadowaki, T., Uesugi, M., Kuznetsov, G., Kumar, N., et al. (2014). Selective inhibition of EZH2 by EPZ-6438 leads to potent antitumor activity in EZH2-mutant non-Hodgkin lymphoma. Mol. Cancer Ther. 13, 842–854.

18. Miranda, T.B., Cortez, C.C., Yoo, C.B., Liang, G., Abe, M., Kelly, T.K., Marquez, V.E., and Jones, P.A. (2009). DZNep is a global histone methylation inhibitor that reactivates developmental genes not silenced by DNA methylation. Mol. Cancer Ther. 8, 1579–1588.

19. Coward, W.R., Feghali-Bostwick, C.A., Jenkins, G., Knox, A.J., and Pang, L. (2014). A central role for G9a and EZH2 in the epigenetic silencing of cyclooxygenase-2 in idiopathic pulmonary fibrosis. FASEB J. 28, 3183–3196.

20. Luli, S., Di Paolo, D., Perri, P., Brignole, C., Hill, S.J., Brown, H., Leslie, J., Marshall, H.L., Wright, M.C., Mann, D.A., et al. (2016). A new fluorescence-based optical imaging method to non-invasively monitor hepatic myofibroblasts in vivo. J. Hepatol. 65, 75–83.

21. Sato, Y., Murase, K., Kato, J., Kobune, M., Sato, T., Kawano, Y., Takimoto, R., Takada, K., Miyanishi, K., Matsunaga, T., et al. (2008). Resolution of liver cirrhosis using vitamin A-coupled liposomes to deliver siRNA against a collagen-specific chaperone. Nat. Biotechnol. 26, 431–442.

22. Li, F., Li, Q.H., Wang, J.Y., Zhan, C.Y., Xie, C., and Lu, W.Y. (2012). Effects of interferon-gamma liposomes targeted to platelet-derived growth factor receptor-beta on hepatic fibrosis in rats. J. Control. Release 159, 261–270.

23. Du, S.L., Pan, H., Lu, W.Y., Wang, J., Wu, J., and Wang, J.Y. (2007). Cyclic Arg-Gly-Asp peptide-labeled liposomes for targeting drug therapy of hepatic fibrosis in rats. J. Pharmacol. Exp. Ther. 322, 560–568.

24. Chai, N.L., Fu, Q., Shi, H., Cai, C.H., Wan, J., Xu, S.P., and Wu, B.Y. (2012). Oxymatrine liposome attenuates hepatic fibrosis via targeting hepatic stellate cells. World J. Gastroenterol. 18, 4199–4206.

25. Wright, M.C., Issa, R., Smart, D.E., Trim, N., Murray, G.I., Primrose, J.N., Arthur, M.J., Iredale, J.P., and Mann, D.A. (2001). Gliotoxin stimulates the apoptosis of human and rat hepatic stellate cells and enhances the resolution of liver fibrosis in rats. Gastroenterology 121, 685–698.

26. Pastorino, F., Stuart, D., Ponzoni, M., and Allen, T.M. (2001). Targeted delivery of antisense oligonucleotides in cancer. J. Control. Release 74, 69–75.

27. Loi, M., Di Paolo, D., Soster, M., Brignole, C., Bartolini, A., Emionite, L., Sun, J., Becherini, P., Curnis, F., Petretto, A., et al. (2013). Novel phage display-derived neuroblastoma-targeting peptides potentiate the effect of drug nanocarriers in preclinical settings. J. Control. Release 170, 233–241.

28. Pastorino, F., Brignole, C., Marimpietri, D., Sapra, P., Moase, E.H., Allen, T.M., and Ponzoni, M. (2003). Doxorubicin-loaded Fab' fragments of anti-disialoganglioside immunoliposomes selectively inhibit the growth and dissemination of human neuroblastoma in nude mice. Cancer Res. 63, 86–92.

29. Di Paolo, D., Pastorino, F., Zuccari, G., Caffa, I., Loi, M., Marimpietri, D., Brignole, C., Perri, P., Cilli, M., Nico, B., et al. (2013). Enhanced anti-tumor and anti-angiogenic efficacy of a novel liposomal fenretinide on human neuroblastoma. J. Control. Release 170, 445–451.

30. Di Paolo, D., Ambrogio, C., Pastorino, F., Brignole, C., Martinengo, C., Carosio, R., Loi, M., Pagnan, G., Emionite, L., Cilli, M., et al. (2011). Selective therapeutic targeting of the anaplastic lymphoma kinase with liposomal siRNA induces apoptosis and inhibits angiogenesis in neuroblastoma. Mol. Ther. 19, 2201–2212.

31. Di Paolo, D., Brignole, C., Pastorino, F., Carosio, R., Zorzoli, A., Rossi, M., Loi, M., Pagnan, G., Emionite, L., Cilli, M., et al. (2011). Neuroblastoma-targeted nanoparticles entrapping siRNA specifically knockdown ALK. Mol. Ther. 19, 1131–1140.

32. Oakley, F., Meso, M., Iredale, J.P., Green, K., Marek, C.J., Zhou, X., May, M.J., Millward-Sadler, H., Wright, M.C., and Mann, D.A. (2005). Inhibition of inhibitor of kappaB kinases stimulates hepatic stellate cell apoptosis and accelerated recovery from rat liver fibrosis. Gastroenterology 128, 108–120.

33. Tam, E.K., Nguyen, T.M., Lim, C.Z., Lee, P.L., Li, Z., Jiang, X., Santhanakrishnan, S., Tan, T.W., Goh, Y.L., Wong, S.Y., et al. (2015). 3-Deazaneplanocin A and neplanocin A analogues and their effects on apoptotic cell death. ChemMedChem 10, 173–182.

34. Liedtke, C., Luedde, T., Sauerbruch, T., Scholten, D., Streetz, K., Tacke, F., Tolba, R., Trautwein, C., Trebicka, J., and Weiskirchen, R. (2013). Experimental liver fibrosis research: update on animal models, legal issues and translational aspects. Fibrogenesis Tissue Repair 6, 19.

35. Pritchard, M.T., and Nagy, L.E. (2005). Ethanol-induced liver injury: potential roles for egr-1. Alcohol. Clin. Exp. Res. 29 (11, Suppl), 146S–150S.

36. Pastorino, F., Marimpietri, D., Brignole, C., Di Paolo, D., Pagnan, G., Daga, A., Piccardi, F., Cilli, M., Allen, T.M., and Ponzoni, M. (2007). Ligand-targeted liposomal therapies of neuroblastoma. Curr. Med. Chem. 14, 3070–3078.

37. Douglass, A., Wallace, K., Parr, R., Park, J., Durward, E., Broadbent, I., Barelle, C., Porter, A.J., and Wright, M.C. (2008). Antibody-targeted myofibroblast apoptosis reduces fibrosis during sustained liver injury. J. Hepatol. 49, 88–98.

38. Elrick, L.J., Leel, V., Blaylock, M.G., Duncan, L., Drever, M.R., Strachan, G., Charlton, K.A., Koruth, M., Porter, A.J., and Wright, M.C. (2005). Generation of a monoclonal human single chain antibody fragment to hepatic stellate cells–a potential mechanism for targeting liver anti-fibrotic therapeutics. J. Hepatol. 42, 888–896.

39. Rius, M., and Lyko, F. (2012). Epigenetic cancer therapy: rationales, targets and drugs. Oncogene 31, 4257–4265.

40. Hinz, B. (2007). Formation and function of the myofibroblast during tissue repair. J. Invest. Dermatol. 127, 526–537.

41. Mann, J., and Mann, D.A. (2013). Epigenetic regulation of wound healing and fibrosis. Curr. Opin. Rheumatol. 25, 101–107.

42. Page, A., Paoli, P.P., Hill, S.J., Howarth, R., Wu, R., Kweon, S.M., French, J., White, S., Tsukamoto, H., Mann, D.A., and Mann, J. (2015). Alcohol directly stimulates epigenetic modifications in hepatic stellate cells. J. Hepatol. 62, 388–397.

43. Mann, J., Oakley, F., Akiboye, F., Elsharkawy, A., Thorne, A.W., and Mann, D.A. (2007). Regulation of myofibroblast transdifferentiation by DNA methylation and MeCP2: implications for wound healing and fibrogenesis. Cell Death Differ. 14, 275–285.

44. Niki, T., Rombouts, K., De Bleser, P., De Smet, K., Rogiers, V., Schuppan, D., Yoshida, M., Gabbiani, G., and Geerts, A. (1999). A histone deacetylase inhibitor, trichostatin A, suppresses myofibroblastic differentiation of rat hepatic stellate cells in primary culture. Hepatology 29, 858–867.

45. Park, K.C., Park, J.H., Jeon, J.Y., Kim, S.Y., Kim, J.M., Lim, C.Y., Lee, T.H., Kim, H.K., Lee, H.G., Kim, S.M., et al. (2014). A new histone deacetylase inhibitor improves liver fibrosis in BDL rats through suppression of hepatic stellate cells. Br. J. Pharmacol. 171, 4820–4830.

46. Liu, Y., Wang, Z., Wang, J., Lam, W., Kwong, S., Li, F., Friedman, S.L., Zhou, S., Ren, Q., Xu, Z., et al. (2013). A histone deacetylase inhibitor, largazole, decreases liver fibrosis and angiogenesis by inhibiting transforming growth factor-β and vascular endothelial growth factor signalling. Liver Int. 33, 504–515.

47. Mannaerts, I., Nuytten, N.R., Rogiers, V., Vanderkerken, K., van Grunsven, L.A., and Geerts, A. (2010). Chronic administration of valproic acid inhibits activation of mouse hepatic stellate cells in vitro and in vivo. Hepatology 51, 603–614.

48. He, S., Barron, E., Ishikawa, K., Nazari Khanamiri, H., Spee, C., Zhou, P., Kase, S., Wang, Z., Dustin, L.D., and Hinton, D.R. (2015). Inhibition of DNA Methylation and Methyl-CpG-Binding Protein 2 Suppresses RPE Transdifferentiation: Relevance to Proliferative Vitreoretinopathy. Invest. Ophthalmol. Vis. Sci. 56, 5579–5589.

49. Feng, Y., Huang, W., Wani, M., Yu, X., and Ashraf, M. (2014). Ischemic preconditioning potentiates the protective effect of stem cells through secretion of exosomes by targeting Mecp2 via miR-22. PLoS ONE 9, e88685.

50. Mayer, S.C., Gilsbach, R., Preissl, S., Monroy Ordonez, E.B., Schnick, T., Beetz, N., Lother, A., Rommel, C., Ihle, H., Bugger, H., et al. (2015). Adrenergic Repression of the Epigenetic Reader MeCP2 Facilitates Cardiac Adaptation in Chronic Heart Failure. Circ. Res. 117, 622–633.

51. Tao, H., Yang, J.J., Hu, W., Shi, K.H., Deng, Z.Y., and Li, J. (2016). MeCP2 regulation of cardiac fibroblast proliferation and fibrosis by down-regulation of DUSP5. Int. J. Biol. Macromol. 82, 68–75.

52. Hu, B., Gharaee-Kermani, M., Wu, Z., and Phan, S.H. (2011). Essential role of MeCP2 in the regulation of myofibroblast differentiation during pulmonary fibrosis. Am. J. Pathol. 178, 1500–1508.

53. Tan, J.Z., Yan, Y., Wang, X.X., Jiang, Y., and Xu, H.E. (2014). EZH2: biology, disease, and structure-based drug discovery. Acta Pharmacol. Sin. 35, 161–174.

54. Völkel, P., Dupret, B., Le Bourhis, X., and Angrand, P.O. (2015). Diverse involvement of EZH2 in cancer epigenetics. Am. J. Transl. Res. 7, 175–193.

55. Kondo, Y. (2014). Targeting histone methyltransferase EZH2 as cancer treatment. J. Biochem. 156, 249–257.

56. Vella, S., Gnani, D., Crudele, A., Ceccarelli, S., De Stefanis, C., Gaspari, S., Nobili, V., Locatelli, F., Marquez, V.E., Rota, R., and Alisi, A. (2013). EZH2 down-regulation exacerbates lipid accumulation and inflammation in in vitro and in vivo NAFLD. Int. J. Mol. Sci. 14, 24154–24168.

57. McGrath, J., and Trojer, P. (2015). Targeting histone lysine methylation in cancer. Pharmacol. Ther. 150, 1–22.

58. Irifuku, T., Doi, S., Sasaki, K., Doi, T., Nakashima, A., Ueno, T., Yamada, K., Arihiro, K., Kohno, M., and Masaki, T. (2015). Inhibition of H3K9 histone methyltransferase G9a attenuates renal fibrosis and retains klotho expression. Kidney Int. 89, 147–157.